Deployable Soft Pneumatic Networks (D-PneuNets) Actuator With Dual-Morphing Origami Chambers for High-Compactness

Woongbae Kim, Bada Seo, Sung Yol Yu, and Kyu-Jin Cho, *Member, IEEE*

***Abstract*—Soft pneumatic networks (PneuNets) actuators are widely considered as a robotic solution for safety and simplicity, yet the trade-off relationship between output force and bulkiness limits usability. In this letter, we propose a deployable soft pneumatic networks (D-PneuNets) actuator consisting of origami-designed chambers. In response to applied pressure, the origami chambers rapidly deploy to increase the moment arm, while simultaneously inflating to bend the whole body through asymmetric lengthening and mutual contacts. Consequently, the D-PneuNets actuator can generate relatively large force, and also provide compactness when not in use. Experiment and finite element analysis results show that the D-PneuNets actuator can grow more than 2.5 times of its initial height, and generate an output force more than 10 times higher compared to that of a conventional soft pneumatic networks actuator with the same initial height. In addition, a dual-material origami chamber with relatively stiff side walls was developed to prevent an unnecessary bulge out. Finally, a robotic soft glove using D-PneuNets actuators was developed and verified for grasping various everyday-objects. Our approach offers a design strategy to overcome the trade-off relationship of soft pneumatic networks actuators, enabling compact designs of soft robotic devices.**

***Index Terms*—Soft actuator, origami-inspired mechanism, deployable mechanism, pneumatic-driven bending actuator, multi-material manufacturing method.**

I. Introduction

SOFT pneumatic actuators have been widely adopted for applications that require delicate interactions with humans or the environment, due to their intrinsic safety originated from soft matters such as elastomers [1], [2], films [3], [4], and fabrics [5]–[8]. The most typical form factor of soft pneumatic bending actuator is the soft pneumatic networks actuator (also widely known as 'PneuNets actuator' [1]). Soft pneumatic networks actuators are in a shape of inflatable chambers arranged in a row (pneumatic networks) above a strain-limiting layer that inextensible flat strip (e.g. paper, fabric, film) is embedded, and they produce continuous bending motion through (i) an asymmetric lengthening of the inextensible layer and extensible pneumatic networks and (ii) mutual contacts between pneumatic chambers. Researchers have developed soft pneumatic networks actuators to be efficient [2], [9]–[11], and applied them to wide range of applications such as robotic grippers [1], [12], wearable devices [10], [13]–[15], and mobile robots [16].

The bulkiness and the output force of the soft pneumatic networks actuator is in a trade-off relationship because the moment produced by extension or interactions of/between the pneumatic chambers is proportional to the square of the height of the chambers [17]. Consequently, to ensure efficient power, the soft pneumatic network actuators are either (i) designed as bulky and highly stretchable silicone beam structures consisting of tall pneumatic chambers [2], [9], [11] or (ii) designed to hold high pressure by making them flexible but less-stretchable by using fabrics [5], [6], [8], thermoplastic polyurethanes (TPUs) [10], [18], or fiber-reinforcement (a method that constrains excessive stretching of materials and guides motion [19], [20]). In the former case (case i), the elastomeric actuators are highly adaptable and actuated in a low pressure range ($<$ 100 kPa). However, the bulkiness limits the compact designs of robotic systems, and may cause inconvenience to users, in applications where physical interactions between human and robot are required, particularly when not in use (e.g. wearable devices). In the latter case (case ii), on the other hand, the actuators can be built in a non-bulky form. However, these actuators require high pressure input ($>$100 kPa) because of the relatively high elastic modulus or because the appendages limit the bending capability. Researchers have enhanced the performance of these actuators by introducing a novel design of pleats for lateral motion [8], [18], yet still not challenging the trade-off relationship of bulkiness and output force that may enhance the performance significantly.

In this paper, we developed a deployable soft pneumatic networks actuator (D-PneuNets) with origami structured pneumatic chambers that can deploy in the height direction. Made of stretchable elastomers, the deployable chambers undergo dual-morphing behavior including early origami-unfolding based morphing and late stretching based morphing, as discovered in our previous study [21]. As a result, the D-PneuNets actuator is

Manuscript received July 28, 2021; accepted November 22, 2021. Date of publication December 23, 2021; date of current version January 6, 2022. This letter was recommended for publication by Associate Editor O. Ozcan and Editor C. Laschi upon evaluation of the reviewers' comments. This work was supported in part by the National Research Foundation of Korea (NRF) under Grant NRF-2016R1A5A1938472 and in part by the Ministry of Trade, Industry and Energy (MOTIE, Korea), through Technology Innovation Program under Grant 20008908. *(Woongbae Kim and Bada Seo contributed equally to this work.) (Corresponding author: Kyu-Jin Cho.)*

The authors are with the Biorobotics Laboratory, Soft Robotics Research Center, SNU-IAMD, Department of Mechanical Engineering, Institute of Engineering Seoul National University, Seoul 08826, Republic of Korea (e-mail: wbae2010@gmail.com; badaroy10@snu.ac.kr; joseph.yu2013@gmail.com; kjcho@snu.ac.kr).

This letter has supplementary downloadable material available at https://doi.org/10.1109/LRA.2021.3137504, provided by the authors.

Digital Object Identifier 10.1109/LRA.2021.3137504

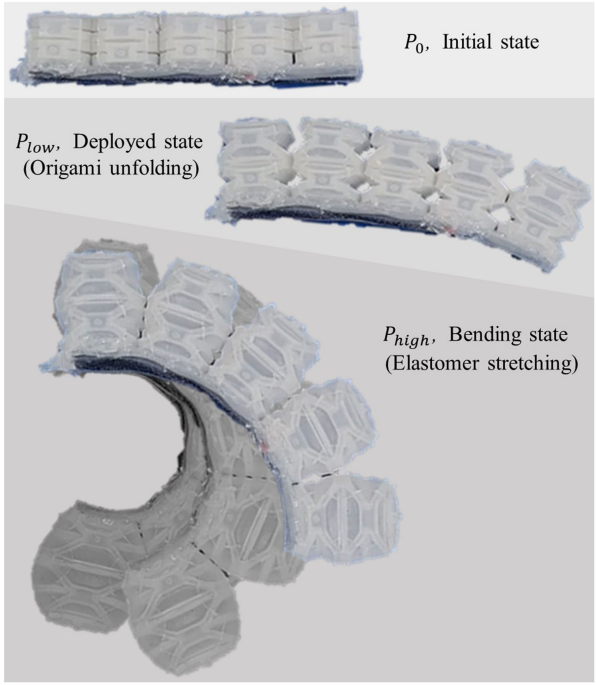

Fig. 1. A D-PneuNets actuator with five Yoshimura origami cylinder structured chambers and its deployment and bending behavior.

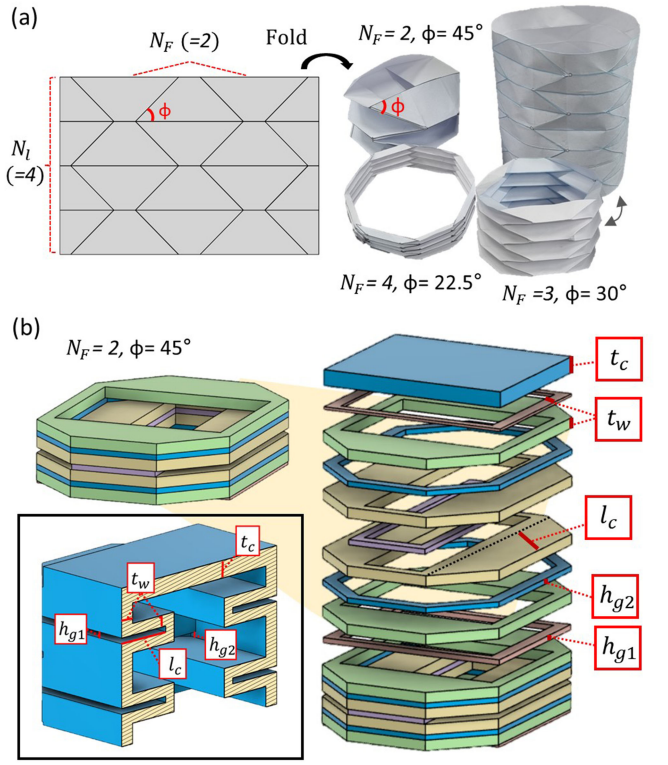

Fig. 2. Yoshimura origami cylinders. (**a**) A paper Yoshimura origami pattern (left) and Paper Yoshimura origami cylinders with N_F= 2, 3, and 4 (right). (**b**) An elastomeric Yoshimura origami cylinder with N_F= 2. An inset image represents a cross-sectional drawing of an elastomeric Yoshimura origami cylinder.

initially in a compact and flat form that the pneumatic chambers are fully folded when not in use, then its chambers grow more than 2.5 times in the height direction to increase the moment arm at a low applied pressure, and finally inflate to generate high force. Our design concept was verified through the comparison of output force with the conventional soft pneumatic networks actuator, and also characterized through experimental study and finite element method (FEM). Using D-PneuNets actuators, we developed a robotic soft glove that is compact when not in use, and demonstrated that it can generate enough power to grip various objects.

The remainder of this paper is organized as follows. In Section II the design and fabrication method are presented. In Section III, a characterization of the D-PneuNets actuators through experiments and simulation results is provided. In Section IV, a robotic soft glove with D-PneuNets is demonstrated. In Section V, the conclusions and future works are presented.

II. Design and Fabrication of the D-PneuNets

A. Design of the D-PneuNets Actuator

The deployment and bending behavior of the D-PneuNets is shown in Fig. 1 and Supplementary Video (the applied pressure was slowly and gradually increased in the video). Its key design difference with the conventional pneumatic networks bending actuator is that the deployable pneumatic chambers are structured as a modified Yoshimura origami cylinders (the triangle tessellation of Yoshimura origami pattern is modified to the trapezoid tessellation, also known as an accordion pattern or a bellows pattern, see Fig. 2(a)) [22]. The radially symmetric pattern guides the origami cylinder to grow linearly. The angle ϕ of the trapezoid tessellation and the number of facets in the same plane when fully folded N_F are in the following relationship:

$$\phi = \frac{90^\circ}{N_F} \tag{1}$$

For the D-PneuNets origami chambers, the minimally complex case of the Yoshimura origami cylinder ($N_F = 2$ and $\phi = 45^\circ$) was chosen because of (i) the potential large deployment ratio by large facets, (ii) the axial symmetry that linearly and symmetrically transmit force, and (iii) relatively simple fabrication comes from the simplicity of the structure with the minimum number of facets. The Yoshimura origami cylinder is not a continuously and rigidly foldable structure (deformation of facets are inevitable for deployment), resulting in a low deployment ratio when made with conventional materials (e.g., papers, fabrics) [23], [24]. However, when the entire structure is built with elastomers, it can fully deploy into a cylindrical structure because the facets can be easily deformed. The fully folded initial height $H_{initial}$ and potential fully unfolded height H_{unfold} of the origami chamber can be defined as follows:

$$H_{initial} = N_l \left(h_{g1} + h_{g2} + 2t_w\right) + t_c \tag{2}$$

$$H_{unfold} = H_{initial} + N_l l_c \tag{3}$$

where N_l, h_{g1}, h_{g2}, t_w, t_c, l_c are the number of layers of the Yoshimura origami pattern, outside gap length between facets,

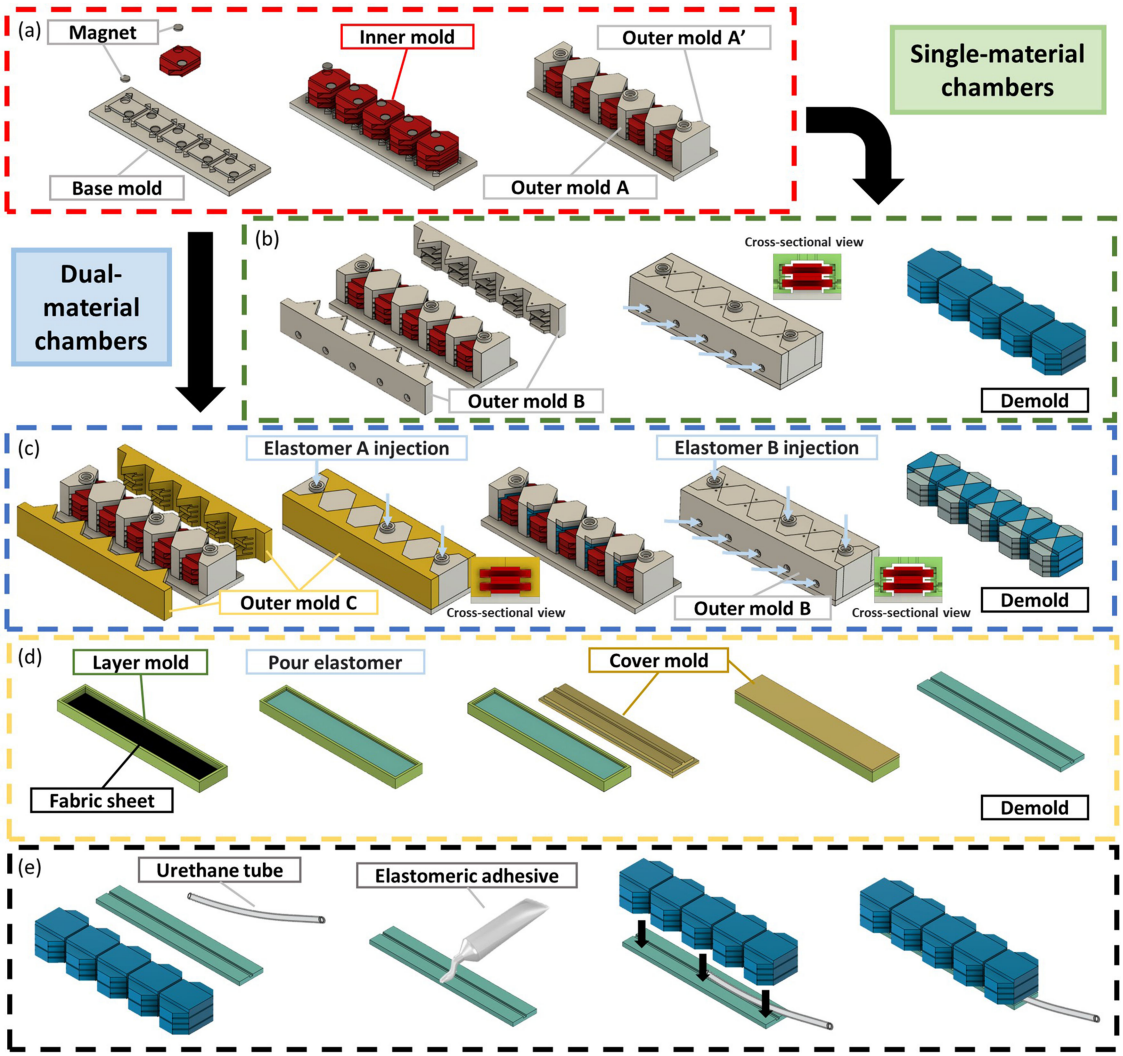

Fig. 3. A schematic diagram of the fabrication process. (**a**) Assembly process of mold using neodymium magnet. (**b**) Fabrication process of the single-material chambers, (**c**) the dual-material chambers, (**d**) the inextensible strain-limiting layer. (**e**) Attachment process of the chambers and the strain-limiting layer.

inside gap length between facets, wall thickness, ceiling thickness, and height of a single tessellation respectively. Therefore, the deployment ratio λ is derived as:

$$\lambda = \frac{H_{unfold}}{H_{initial}} = 1 + \frac{N_l l_c}{H_{initial}} \tag{4}$$

When the pneumatic pressure is applied into the elastomeric origami chambers, both unfolding and stretching occurs simultaneously [21]. At a low applied pressure level, however, the unfolding is the dominant morphing behavior and the elastomeric Yoshimura origami cylinders mainly grow in the height direction. As the origami structures are almost unfolded, the dominant morphing behavior shifts from unfolding to stretching and the entire body inflates. Consequently, the D-PneuNets actuators undergo deployment and bending where (i) the origami chambers grow in the height direction, getting ready to generate high power, and (ii) the origami chambers inflate and bending the entire actuator. Bending is produced by the strain difference between the inflating chambers and the strain-limiting layer, in addition to the mutual contacts that occur from the chambers pushing against each other. It is also notable that unfolding proceeds rapidly from the beginning of actuation and is almost completed at a certain pressure, but bending occurs throughout the actuation process.

B. Fabrication

Molding and casting is the most general fabrication method for elastomeric soft robots [25]. For complex structures such as origami structures, however, a detaching process of the mold may require too much effort. In addition, the mold may have to be sacrificed by breaking or melting. [26]. In our previous research, for example, a stacking of the water-soluble polyvinyl alcohol (PVA) molds was proposed to fabricate the elastomeric origami structures [21]. Because the sacrificial molds are not reusable, the processes were time and cost consuming compared to the general molding and casting process.

To solve this issue, we designed inner molds to be easily assembled and disassembled through magnetic force. As shown in Fig. 3(a), neodymium disc magnets were fitted inside the

holes of the base molds and the inner molds. After the elastomers are cured, the inner molds can be disassembled and pulled out from inside the elastomeric origami chambers part by part, instead of sacrificing them. All molds were 3D printed by Objet 260 Connex3 (Stratasys Ltd.) using a rigid material VeroWhitePlus$^{\mathrm{TM}}$(shore hardness 85D, Stratasys, Ltd.).

The fabrication process of the D-PneuNets actuators is shown in Fig. 3. Similar to the fabrication process of the conventional soft pneumatic bending actuators, the extensible fluidic networks and the inextensible strain-limiting layer are fabricated separately, and are bonded in the final process. The fabrication process of the pneumatic networks is shown in Fig. 3(a) and (b). First, neodymium disc magnets were assembled to the base mold and the inner molds, and the inner molds were stacked on top of the base mold. Secondly, the outer molds (A, A' and B) were assembled in sequence. At this time, the outer molds A and A' were aligned along the triangularly shaped bulges of the base mold. Finally, an elastomer, Dragon Skin10 (shore hardness A 10, Smooth-on Inc.) or Dragon Skin30 (shore hardness A 30, Smooth-on Inc.), was injected through the holes of the outer molds, cured in an oven at 75 °C for 1 h, and the molds were disassembled in the reverse order. In the preparation process, elastomers were colored using silicone color pigments Silc Pig$^{\mathrm{TM}}$(Smooth-on Inc.) to be distinguished.

We also developed a fabrication process for dual-material chambers as shown in Fig. 3(c) (the purpose of the dual-material chamber is discussed in Section III-C). After the process shown in Fig. 3(a), the outer mold C with no gaps between the inner molds was assembled, and Dragon Skin30 was injected through the outer molds A and A' and half-cured in the oven at 75 °C for 15 minutes. The half-cured elastomer hardens and retains its shape, but still can adhere to uncured elastomers. Then, the outer mold C was replaced by outer mold B and Dragon Skin10 was injected through the outer mold B. After cured in the oven at 75 °C for 6 hours, the molds were disassembled.

The inextensible strain-limiting layers were fabricated as shown in Fig. 3(d) and were attached with the pneumatic networks as shown in Fig. 3(e). An elastomeric adhesive (Sil-poxy$^{\mathrm{TM}}$, Smooth-on Inc.) was applied flawlessly on the strain-limiting layer, the pneumatic network was placed on it. Finally, 1.8-mm-diameter polyurethane tube (MPUT1.8-10-C, MISUMI) was inserted at the end, and the actuator was cured in the oven at 75 °C for 10 minutes.

III. Characterization of the Actuator

A. Concept Validation

Based on the moment equilibrium and Hertzian contact theory, Zhu Liu *et al.* established a tip force model of the soft pneumatic networks actuator [17]. Assuming that the thickness of the strain-limiting layer is small enough to be neglected, the tip force model is express as follow:

$$F_t = \frac{Pw\,(n-1)\,(7-4\alpha)}{2\,\{nl+(n-1)\,l_g\}}H^2 \tag{5}$$

where P, w, n, l, l_g, α, and H are the applied pressure, the width of the chamber, the number of the chambers, the the length of single chamber, the gap length, the coefficient related to Hertzian contact and the height of the chamber, respectively. Given the relationship $F_t \sim H^2$, the D-PneuNets actuators can generate an output force of $(\frac{H_{unfold}}{H_{initial}})^2$ times compared to the conventional soft pneumatic networks actuators with chamber height of $H_{initial}$.

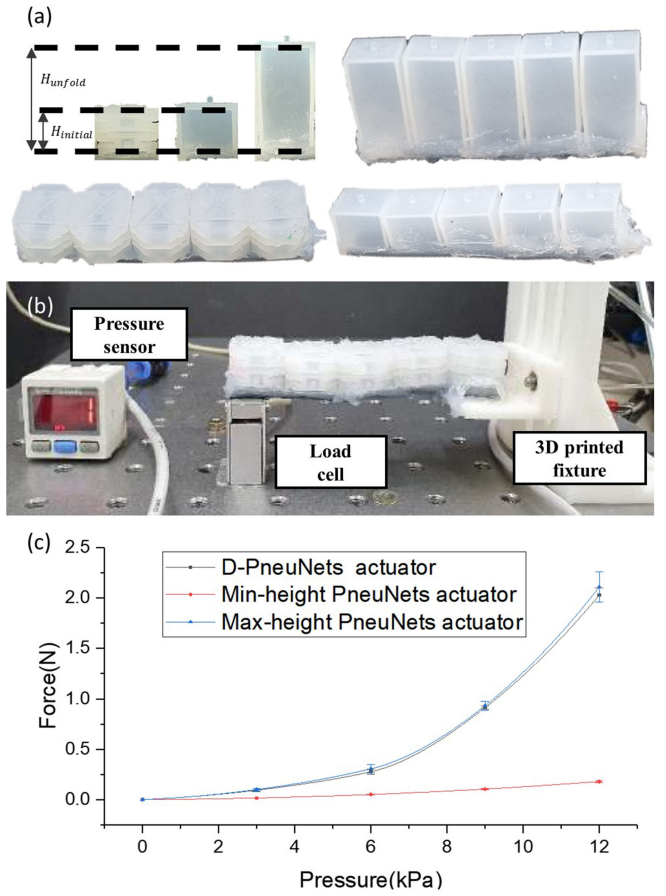

Fig. 4. A force measurement experiment. (**a**) D-PneuNets and two soft pneumatic network actuators with each height equal to $H_{initial}$ and H_{unfold}. (**b**) An experimental setup for force measurement. (**c**) An experimental result of the force measurement.

To validate the design concept, we measured the output forces of a D-PneuNets actuator and two soft pneumatic network actuators with each height equal to the initial height ($H_{initial}$) and fully unfolded height (H_{unfold}) of the D-PneuNets actuator (we call them Min-height PneuNets actuator and Max-height-PneuNets actuator respectively). The actuators are shown in Fig. 4(a) (five chambers), and all of them were built with Dragon Skin 10. In order for the conditions to be as similar as possible, the corresponding design parameters between the D-PneuNets actuator ($N_l = 4$, h_{g1}= 0.5 mm, h_{g2}= 0.5 mm, t_w= 1 mm, t_c= 1.5 mm and l_c= 5.25 mm) and the conventional actuators were all designed to be the same (e.g., wall thickness). The initial and unfolded height of the origami deployable chambers were $H_{initial} = 13.5\,mm$ and $H_{unfold} = 34.5\,mm$, which is a 2.56 fold growth. The experimental setup is shown in Fig. 4(b); the tip of the actuator was positioned at the top of the load cell (333FDX,

KTOYO), and the tip force at a zero bending angle was measured at an applied pneumatic pressure from 0 kPa to 12 kPa in 3 kPa increments, regulated by a pressure regulator (RVUM, PISCO). For each actuator, the experiment was performed 5 times.

The experimental result is shown in Fig. 4(c). The output forces of the D-PneuNets actuator and the Max-height-PneuNets actuator were measured almost equally within the error range. At 12 kPa, the average output forces of the D-PneuNets actuator and Max-height-PneuNets actuator were 2.023 N and 2.109 N, respectively. On the other hands, the Min-height-PneuNets actuator only generated an average output force of 0.178 N at an applied pneumatic pressure of 12 kPa, which is significantly lower (<10 %) than the D-PnueNets actuator of the same initial chamber height. The experimental result, therefore, verifies the design concept of the D-PnueNets actuator, which is compact when not in use and capable of generating large force when required.

B. Characterization of the Behavior

Parametric studies regarding unfolding and stretching behaviors of elastomeric origami chambers were studied in our previous study [21]; as the widths of the crease lines decrease, the unfolding response becomes more sensitive to applied pneumatic pressure while the stretching response of the material does not change. In this work, we have further investigated whether the unfolding behavior of the origami chambers affects the bending behavior of the actuator.

Two D-PneuNets actuators with three chambers, made of Dragon Skin30, with l_g of 1 mm and 3 mm, respectively, were prepared. As experimental setup shown in Fig. 5(a), the actuators were hung on a stand and red circle markers were attached. A pneumatic pressure was applied from 0 kPa to 30 kPa in 3 kPa increments, and frontal photographs were taken for every steps. Using Matlab code, the position of the markers were found (MATLAB function 'imfindcircles' was utilized). Using the position data, the radius of the arc-shaped strain-limiting layer R and the change in chamber height ΔH were calculated.

A finite element analysis (FEA) was conducted using a software ABAQUS (Dassault systems) as shown in Fig. 5(b). In order to reduce computational complexity that increase run time and may cause non convergence problems, models divided into quarters with respect to a symmetrical plane were imported and boundary conditions corresponding to the symmetry conditions were set. Uniaxial and biaxial test results of the elastomers were imported to ABAQUS and fitted as Ogden 3 rd order hyperelastic model. All analysis were conducted under quasi-static condition and penalty contact method. FEA of conventional pneumatic networks actuators were also conducted in addition to FEA of the D-PneuNets actuators for comparison.

Experimental and simulation results for bending curvature of the actuators ($\kappa = 1/R$) and the height change of the chambers (ΔH) in response to applied pneumatic pressure are shown in Fig. 5(c) and (d), respectively. For all actuators, κ increased slowly before the mutual contact (<3 kPa) but increased rapidly after the interaction between chambers began (>3 kPa). For example, for the D-PneuNets actuator with l_g= 3 mm, κ was

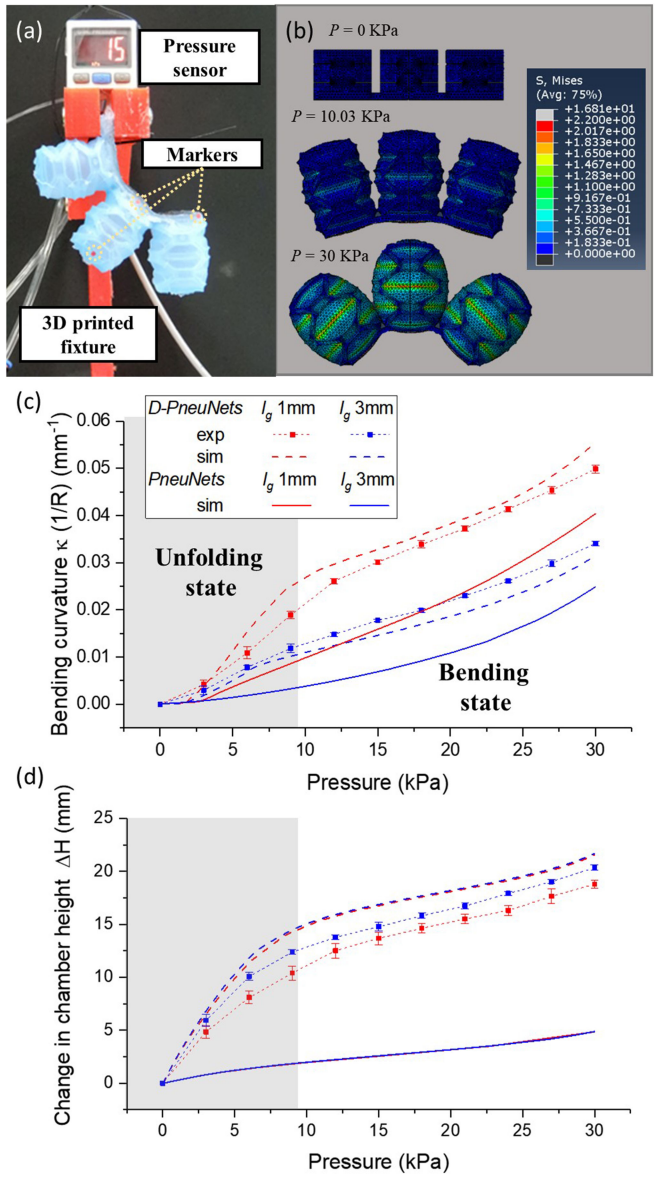

Fig. 5. The deployment and bending behavior of a D-PneuNets actuator. (**a**) An experimental setup to measure the deployment and bending behavior. (**b**) FEA simulation results of the D-PneuNets actuator with $l_g = 3$ mm. (**c** and **d**) Experimental and simulation result (**c**) of the curvature κ and (**d**) the change in chamber height ΔH for the actuators with $l_g = 1$ mm and 3 mm.

0.00295 at 3 kPa and increased to 0.0118 at 9 kPa. Also, naturally, κ of the D-PneuNets actuator with $l_g = 1$ mm was larger than for $l_g = 3$ mm (from 39% to 77%) due to the effect of the mutual contact.

Particularly noteworthy, the gradient of κ for the D-PneuNets actuators is large during unfolding phase after the mutual contact (3 kPa<P<9 kPa), and then the gradient decreases as the chambers are mostly unfolded (P>12 kPa). For the conventional pneumatic networks actuators, on the other hands, the gradient of κ gradually increases as pressure is applied. This seems to be because the crease lines of the D-PneuNets actuators protrude in side directions during the unfolding process, causing a large interaction between the chambers. Consequently, the

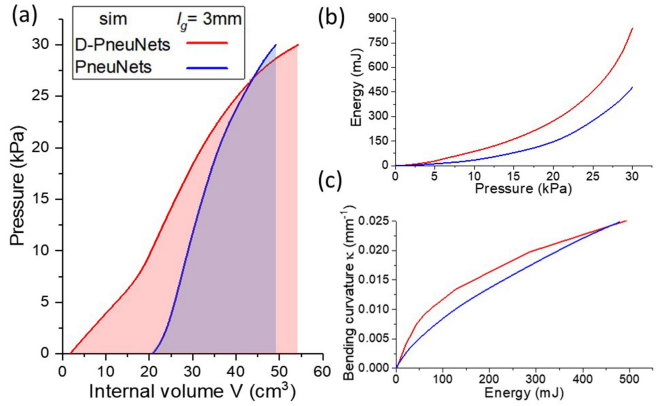

Fig. 6. (**a**) Simulation results of the D-PneuNets and PneuNets actuators for the internal volume and (**b**) the stored energy to applied pressure. (**c**) The relationship between stored energy and bending curvature.

D-PneuNets actuators significantly bent more than the conventional pneumatic networks actuators. For example, for the simulation results of the D-PneuNets actuator and the pneumatic networks actuator with $l_g = 1$ mm, κ at 22.5 kPa were 0.0411 and 0.0266, respectively.

For ΔH, the D-PneuNets actuator with $l_g = 3$ mm was slightly larger for $l_g = 1$ mm. The result is probably because the interaction between the chambers inhibits the unfolding. In addition, ΔH of the conventional pneumatic networks actuators increased as the chambers were stretched, but the amount was much lower than the D-PneuNets actuators deployed by unfolding at a low pressure; simulation results of $l_g = 3$ mm actuators for ΔH at 30 kPa were 21.54 mm and 4.88 mm, respectively.

The simulation results of the D-PneuNets actuator and the PneuNets actuator (chamber height of H_{unfold})'s internal volumes (V) in response to applied pressure are shown in Fig. 6(a). Due to the overlap of the unfolding and stretching, V of the D-PneuNets actuator increases rapidly from 1.73 cm^3 to 54.29 cm^3, compared to V of the PneuNets actuator with only stretching increases from 20.76 cm^3 to 49.17 cm^3, for an applied pressure of 30 kPa. From the result, the stored energy ($E = \int PdV$) to the applied pressure was calculated, and result shows that E of the D-PneuNets actuator was higher (more than 1.7 times) than PneuNets actuator at the same applied pressure (Fig. 6(b)). On the other hand, there was no notable difference in required energy for bending, especially after being fully unfolded, as shown in Fig. 6(c).

C. Dual-Material Yoshimura Origami Cylinder Chamber

The chamber side walls of conventional pneumatic networks actuators are designed to be thicker than the front and back walls [2], or undesired bulge outs of the chamber occur in areas where mutual contact does not occur. However, for the D-PneuNets origami chambers, $H_{initial}$ increases as the side wall thickness t_w increases, resulting in a decrease in λ (see equations (2) and (4)). Instead of thickening the side walls, we applied a dual material design to increase the stiffness of the side walls. As shown in Fig. 7(a), the chamber was divided into 4 sections in the shape of an X when viewed from above, and

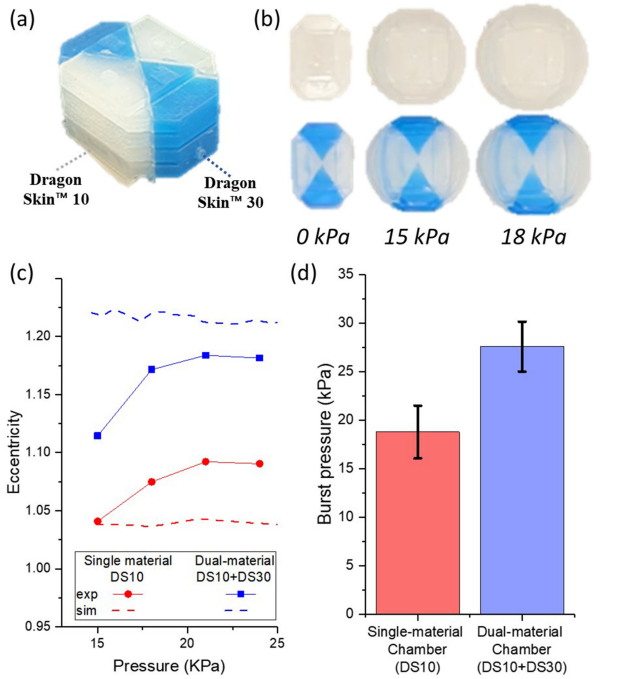

Fig. 7. A Dual-material Yoshimura origami cylinder chamber. (**a**) A material composition of the dual-material chamber. (**b**) Dual-material origami chambers viewed from above. (**c**) Experimental and simulation results for the eccentricity of the origami chambers. (d) Experimental results for the bust pressure of the origami chambers.

Dragon Skin30 was applied to two sections corresponding to the side walls while Dragon Skin10 was applied to the rest of the sections.

The shape changes of the single-material chamber and the dual-material chamber were measured. From 12 kPa to 24 kPa in 3 kPa increments, a pneumatic pressure was applied and the top view photographs were taken as shown in Fig. 7(b); low pressure was excluded because the chambers did not expand sufficiently enough. The shape of the inflated chambers viewed from above was assumed as an ellipse. Using MATLAB code, the boundaries were found and eccentricities were calculated. FEA was also conducted and analyzed in the same process.

Experimental and simulation results of eccentricity in response to the applied pressure is shown in Fig. 7(c). As intended, the lateral bulge out of the dual-material chamber was mitigated compared to the single-material chamber. The eccentricities were 1.18 and 1.09 at 21 kPa for the dual-material chamber and single-material chamber respectively. Compared to the simulation result, the experimental result shows smaller difference in eccentricity between the single-material chamber and the dual-material chamber, which is presumably due to the unintentional mixing of materials between half-cured Dragon Skin10 and injected Dragon Skin30 during the fabrication process.

The burst pressures of the single-material chambers (Dragonskin 10) and the dual-material chambers were measured as shown in Fig. 7(d). Five chambers were tested for each type, and the average burst pressure were 18.8 kPa and 27.6 kPa for the single-material chambers and the dual-material chambers, respectively. For the single-material chambers, the burst

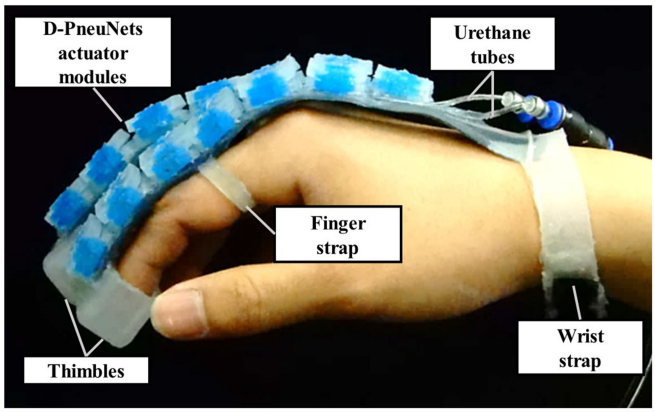

Fig. 8. A prototype of the D-PneuNets soft robotic glove.

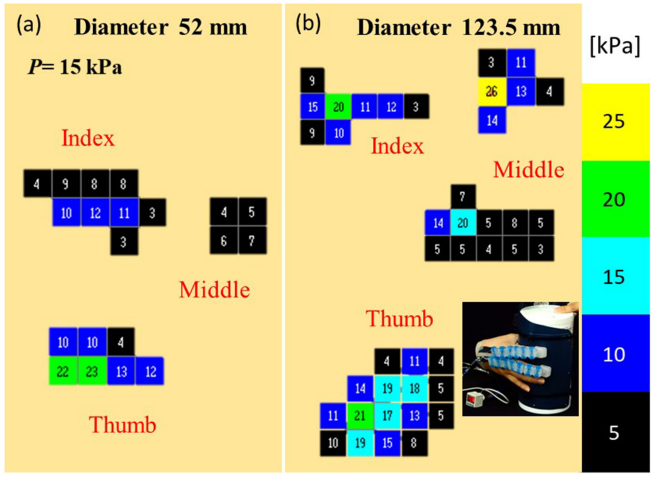

Fig. 9. Wrap grasping pressure measurement results for cylindrical objects of (**a**) diameter = 65 mm and (**b**) diameter = 140 mm.

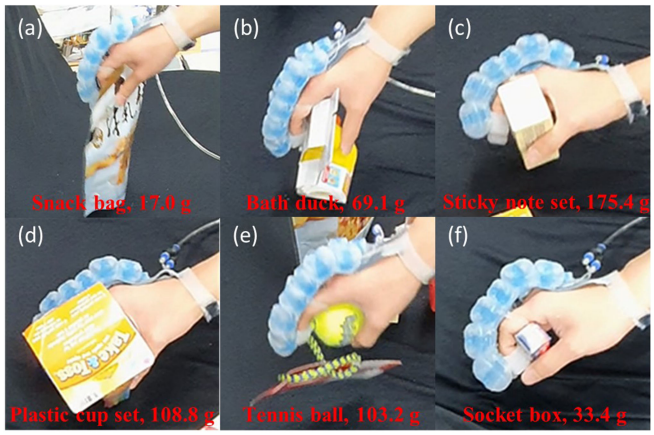

Fig. 10. Grasping tests with various objects. (**a**) Snack bag, (**b**) bath duck, (**c**) Sticky note set, (**d**) plastic cup set, (**e**) tennis ball, and (**f**) socket box.

occurred at random locations. On the other hands, for the dual-material chambers, the burst occurred at the boundary of the two materials.

IV. Robotic Soft Glove Using D-PneuNets Actuators

For the purpose of assisting and rehabilitating hand motor functions of stroke patients, researchers have been developed robotic gloves that bend fingers [14], [15], [27]–[29]. In particular, robotic soft gloves using soft pneumatic actuators provide not only inherent safety but also simplicity to users that comes from no need of rigid components or complicated routing, compared to linkage-based mechanisms [30] and tendon-driven mechanisms [28], [29], respectively. These advantages offer the potential of greatly improving the activities of daily living (ADL).

A soft robotic glove prototype using D-PneuNets actuators was developed as shown in Fig. 8. Due to the deployable actuator, the developed soft robotic glove provides initial compactness while generating sufficient force when in use. Two D-PneuNets actuators wrap over the index and middle fingers (six and seven chambers, respectively) and fastened by elastomeric thimbles, finger straps, and a wrist strap. All elastomeric components were fabricated in a single step by molding and casting, using 3D printed molds. The dual-material chambers with $N_l = 2$ ($H_{initial} = 6.75$ mm) were chosen for compactness. Air was applied to both actuators simultaneously through urethane tubes using an external pneumatic source. The glove part is entirely soft, water-proof, and light-weight, weighing 71.2 g.

An experiment to measure pressure distribution of the D-PneuNets soft robotic glove during wrap grasping was conducted. A mat-type pressure sensor Pliance (Novel Inc.) was wrapped around two cylindrical objects with diameters of 52 mm and 123.5 mm. After sensor calibration, the wearer wrapped the objects with his hand relaxed, and then 20 kPa of pneumatic pressure was applied to the D-PneuNets soft robotic glove. The result is shown in Fig. 9(a) and (b); the D-PneuNets soft robotic glove generated 4.75 N and 11.76 N for diameter of 52 mm and 123.5 mm cylinders, respectively. The measured pressure was distributed as low values due to the softness of the glove and human hand. Assuming the friction coefficient of Dragon Skin30 as 0.8 [31], it can be concluded that the D-PneuNets soft robotic glove can hold up to weight of 960 g by applying only 20 kPa of pneumatic pressure.

Finally, we conducted a grasping test with the D-PneuNets soft robotic glove for six everyday-objects as shown in Fig. 10 and Supplementary Video. Objects of various shapes (pouch, ball, cylinder, boxes, etc.) and weights (from 17 g to 175 g) were moved and placed by a subject wearing the D-PneuNets soft robotic glove with the same applied pneumatic pressure of 20 kPa. It took about 60 seconds to move the six objects, and all objects were held stably without slip or wobble.

V. Conclusion

In this letter, a new type of soft pneumatic networks bending actuator utilizing deployable origami-shaped chambers was proposed, to generate high force compared to the compact initial form. Both behaviors of the actuator and the inflation of chambers, including dual-material chamber for preventing unnecessary bulge out, were characterized by experiment and FEA simulation. As an application, a prototype of the robotic soft glove using D-PneuNets actuators was developed. The

experiment and demonstration confirmed that the developed robotic glove provides sufficient performance to grab various everyday-objects, with advantages of having an initial compact form and low actuation pressure. Despite the complex origami structure, the D-PneuNets actuators could be fabricated by molding and casting with the help of magnet assembly/disassembly of inner molds.

Future works for D-PneuNets actuator include analytic or numerical modelling to estimate both the morphing of chambers and the bending of the strain-limiting layer. For the D-PneuNets soft robotic glove, building the entire system including a controller and a power source (e.g., a pneumatic supply system presented in [32]) and evaluating the usability and durability are required. As for the fabrication method that enables mold reconfiguration and multi-material placement, we expect it to be utilized in the manufacturing of multi-functional soft robots. We believe our approach offers a new design method for compact and space-efficient pneumatic soft actuators that can also be implemented in various materials (e.g., fabrics and TPUs), and can be applied to portable, mobile, or wearable robotic applications.

REFERENCES

[1] F. Ilievski, A. D. Mazzeo, R. F. Shepherd, X. Chen, and G. M. Whitesides, "Soft robotics for chemists," *Angewandte Chemie*, vol. 123, no. 8, pp. 1930–1935, 2011.

[2] B. Mosadegh *et al.*, "Pneumatic networks for soft robotics that actuate rapidly," *Adv. Funct. Mater.*, vol. 24, no. 15, pp. 2163–2170, 2014.

[3] R. Niiyama, X. Sun, C. Sung, B. An, D. Rus, and S. Kim, "Pouch motors: Printable soft actuators integrated with computational design," *Soft Robot.*, vol. 2, no. 2, pp. 59–70, 2015.

[4] H. Sareen *et al.*, "Printflatables: Printing human-scale, functional and dynamic inflatable objects," in *Proc. CHI Conf. Hum. Factors Comput. Syst.*, 2017, pp. 3669–3680.

[5] R. F. Natividad, M. R. D. Rosario, P. C. Chen, and C. H. Yeow, "A hybrid plastic-fabric soft bending actuator with reconfigurable bending profiles," in *Proc. IEEE Int. Conf. Robot. Automat.*, 2017, pp. 6700–6705.

[6] P. H. Nguyen and W. Zhang, "Design and computational modeling of fabric soft pneumatic actuators for wearable assistive devices," *Sci. Rep.*, vol. 10, no. 1, pp. 1–13, 2020. [Online]. Available: http://dx.doi.org/10.1038/s41598-020-65003-2

[7] H. J. Yoo *et al.*, "Wearable lymphedema massaging modules: Proof of concept using origami-inspired soft fabric pneumatic actuators," in *Proc. IEEE 16th Int. Conf. Rehabil. Robot.*, 2019, pp. 950–956.

[8] L. Cappello *et al.*, "Exploiting textile mechanical anisotropy for fabric-based pneumatic actuators," *Soft Robot.*, vol. 5, no. 5, pp. 662–674, 2018.

[9] X. Ke *et al.*, "Stiffness preprogrammable soft bending pneumatic actuators for high-efficient, conformal operation," *Soft Robot.*, ahead of Print, 2021.

[10] B. W. Ang and C. H. Yeow, "Design and modeling of a high force soft actuator for assisted elbow flexion," *IEEE Robot. Automat. Lett.*, vol. 5, no. 2, pp. 3731–3736, Apr. 2020.

[11] H. T. D. Chun, J. O. Roberts, M. E. Sayed, S. Aracri, and A. A. Stokes, "Towards more energy efficient pneumatic soft actuators using a port-hamiltonian approach," in *Proc. 2nd IEEE Int. Conf. Soft Robot.*, 2019, pp. 277–282.

[12] Z. Wang, Y. Torigoe, and S. Hirai, "A prestressed soft gripper: Design, modeling, fabrication, and tests for food handling," *IEEE Robot. Automat. Lett.*, vol. 2, no. 4, pp. 1909–1916, Oct. 2017.

[13] Z. Wang and S. Hirai, "Soft gripper dynamics using a line-segment model with an optimization-based parameter identification method," *IEEE Robot. Automat. Lett.*, vol. 2, no. 2, pp. 624–631, Apr. 2017.

[14] J. Wang, Y. Fei, and W. Pang, "Design, modeling, and testing of a soft pneumatic glove with segmented PneuNets bending actuators," *IEEE/ASME Trans. Mechatronics*, vol. 24, no. 3, pp. 990–1001, Jun. 2019.

[15] P. Polygerinos *et al.*, "Towards a soft pneumatic glove for hand rehabilitation," in *Proc. IEEE/RSJ Int. Conf. Intell. Robots Syst.*, 2013, pp. 1512–1517.

[16] R. F. Shepherd *et al.*, "Multigait soft robot," *Proc. Nat. Acad. Sci. United States Amer.*, vol. 108, no. 51, pp. 20400–20403, 2011.

[17] Z. Liu, F. Wang, S. Liu, Y. Tian, and D. Zhang, "Modeling and analysis of soft pneumatic network bending actuators," *IEEE/ASME Trans. Mechatronics*, vol. 26, no. 4, pp. 2195–2203, Aug. 2020.

[18] B. A. W. Keong and R. Y. C. Hua, "A novel fold-based design approach toward printable soft robotics using flexible 3D printing materials," *Adv. Mater. Technol.*, vol. 3, no. 2, pp. 1–12, 2018.

[19] P. Polygerinos, Z. Wang, K. C. Galloway, R. J. Wood, and C. J. Walsh, "Soft robotic glove for combined assistance and at-home rehabilitation," in *Proc. Robot. Auton. Syst.*, 2015, vol. 73, pp. 135–143.

[20] K. H. Heung, R. K. Tong, A. T. Lau, and Z. Li, "Robotic glove with soft-elastic composite actuators for assisting activities of daily living," *Soft Robot.*, vol. 6, no. 2, pp. 289–304, 2019.

[21] W. Kim *et al.*, "Bioinspired dual-morphing stretchable origami," *Sci. Robot.*, vol. 4, no. 36, 2019, Art. no. eaay3493.

[22] Y. Yoshimaru, "On the mechanism of buckling of a circular cylindrical shell under axial compression," Tech. Memorandum 1390, National Advisory Committee for Aeronautics, Washington, DC, USA, 1955.

[23] K. Miura and T. Tachi, "Synthesis of rigid-foldable cylindrical polyhedra," in *Symmetry: Art Sci.*, 2010, pp. 204–213.

[24] J. E. Suh, T. H. Kim, and J. H. Han, "New approach to folding a thin-walled Yoshimura patterned cylinder," *J. Spacecraft Rockets*, vol. 58, no. 2, pp. 516–530, 2021.

[25] P. Polygerinos *et al.*, "Soft robotics: Review of fluid-driven intrinsically soft devices; Manufacturing, sensing, control, and applications in human-robot interaction," *Adv. Eng. Mater.*, vol. 19, no. 12, 2017, Art no. 1700016.

[26] A. Koivikko and V. Sariola, "Fabrication of soft devices with buried fluid channels by using sacrificial 3D printed molds," in *Proc. 2nd IEEE Int. Conf. Soft Robot.*, Seoul, 2019, pp. 509–513.

[27] S. S. Yun, B. B. Kang, and K. J. Cho, "Exo-glove PM: An easily customizable modularized pneumatic assistive glove," *IEEE Robot. Automat. Lett.*, vol. 2, no. 3, pp. 1725–1732, Jul. 2017.

[28] H. In, B. B. Kang, M. K. Sin, and K. J. Cho, "Exo-glove: A wearable robot for the hand with a soft tendon routing system," *IEEE Robot. Automat. Mag.*, vol. 22, no. 1, pp. 97–105, Mar. 2015.

[29] L. Gerez, J. Chen, and M. Liarokapis, "On the development of adaptive, tendon-driven, wearable exo-gloves for grasping capabilities enhancement," *IEEE Robot. Automat. Lett.*, vol. 4, no. 2, pp. 422–429, Apr. 2019.

[30] T. T. Worsnopp, M. A. Peshkin, J. E. Colgate, and D. G. Kamper, "An actuated finger exoskeleton for hand rehabilitation following stroke," in *Proc. IEEE 10th Int. Conf. Rehabil. Robot.*, 2007, pp. 896–901.

[31] Z. Wang, R. Kanegae, and S. Hirai, "Circular shell gripper for handling food products," *Soft Robot.*, vol. 8, no. 25, pp. 542–554, 2020.

[32] S. Joshi and J. Paik, "Pneumatic supply system parameter optimization for soft actuators," *Soft Robot.*, vol. 8, no. 2, pp. 152–163, 2021.